nature structural & molecular biology

Mechanochemical coupling of two substeps in a single myosin V motor

Sotaro Uemura[1], Hideo Higuchi[2,3], Adrian O Olivares[4], Enrique M De La Cruz[4] & Shin'ichi Ishiwata[1,5]

Myosin V is a double-headed processive molecular motor that moves along an actin filament by taking 36-nm steps. Using optical trapping nanometry with high spatiotemporal resolution, we discovered that there are two possible pathways for the 36-nm steps, one with 12- and 24-nm substeps, in this order, and the other without substeps. Based on the analyses of effects of ATP, ADP and 2,3-butanedione 2-monoxime (a reagent shown here to slow ADP release from actomyosin V) on the dwell time and the occurrence frequency of the main and the intermediate states, we propose that the 12-nm substep occurs after ATP binding to the bound trailing head and the 24-nm substep results from a mechanical step following the isomerization of an actomyosin-ADP state on the bound leading head. When the isomerization precedes the 12-nm substep, the 36-nm step occurs without substeps.

Myosin V belongs to the myosin superfamily of actin-based molecular motors and is involved in the intracellular transport of organelles[1–4]. Myosin V consists of two identical heavy chains, each composed of an N-terminal motor domain ('head'), a domain comprising six IQ motifs that bind light chains ('neck'), a coiled coil dimerization domain and a globular cargo-binding tail domain[1,3]. Myosin V is a processive motor that 'walks' along an actin filament toward the barbed end over a long distance without dissociating from the filament[5,6]. Electron microscopy of actomyosin V in the presence of low ATP concentrations shows both motor domains of myosin V bound to the actin filament at sites spaced 36 nm apart, which corresponds to the half pitch of the filament long-pitch helix[7]. Experiments using optical tweezers identified processive 36-nm steps of a bead, on which single myosin V molecules were adsorbed[6,8]. Moreover, it was shown that myosin V walks as a left-handed spiral motor along an actin filament, because the average step size is slightly shorter than the half pitch of the long-pitch actin helix[9].

The hand-over-hand walking model has received strong support from two recent experiments that (i) observed the orientation of the neck domain of myosin V by monitoring the polarization of a single fluorophore covalently attached to a light chain[10] and (ii) measured the stepwise displacement of a single fluorophore labeled at one of six light chains of myosin V[11].

Solution kinetic studies demonstrate that ADP release occurs at ~15 s^{-1} and limits the myosin V ATPase cycle[12]. Microscopic analysis of myosin V stepping under various nucleotide conditions is consistent with rate-limiting ADP release[13]. The next key target is to determine how the mechanical and biochemical cycles are coupled to each other at the single-molecule level.

Here, we focused on mechanical events and detected substeps that occur within each regular 36-nm step with high temporal resolution. Each regular 36-nm step is composed of two consecutive substeps, one generating a 12-nm substep and the other a 24-nm substep. To investigate how these substeps and the states attained after the steps are coupled to the ATPase cycle of myosin V, we examined the effects of ATP and ADP concentrations, and 2,3-butanedione 2-monoxime (BDM)[14]. We also examined the force dependence of the occurrence frequency of each step and substep, and the dwell time of each state.

RESULTS

Movement of myosin V along an actin filament

A single myosin V–coated bead was trapped with optical tweezers and brought into contact with a fluorescently labeled biotinylated actin filament, which was immobilized on an avidin-coated glass surface through biotinylated BSA (**Fig. 1a**). A focused red light (685 nm) laser was used to diagonally illuminate the bead, and its dark-field image was projected onto a quadrant photodiode. The bead displacement was determined by measuring the differential output of the quadrant photodiode with nanometer accuracy and a 10-kHz sampling rate[15]. The use of a 200-nm-diameter bead here instead of a 1-μm bead was essential to obtain a high spatiotemporal resolution.

An example of the time course of bead displacement along an actin filament (**Fig. 1b**) shows three consecutive runs of a single myosin V molecule along an actin filament at a saturating ATP concentration (1 mM). As the bead began to deviate from the trap center, a positive external load was applied to the myosin V–actin complex (toward the pointed end of an actin filament). Myosin V detached from actin at a stall force of ~3 pN. After detachment, the bead quickly returned to the

[1]Department of Physics, School of Science and Engineering, Waseda University, 3-4-1 Okubo, Shinjuku-ku, Tokyo 169-8555, Japan. [2]Department of Metallurgy, Graduate School of Engineering, [3]Center of Interdisciplinary Research, Tohoku University, Sendai, 980-8579, Japan. [4]Department of Molecular Biophysics and Biochemistry, Yale University, New Haven, Connecticut 06520, USA. [5]Advanced Research Institute for Science and Engineering, Waseda University, 3-4-1 Okubo, Shinjuku-ku, Tokyo 169-8555, Japan. Correspondence should be addressed to S.I. (ishiwata@waseda.jp).

Published online 1 August 2004; doi:10.1038/nsmb806

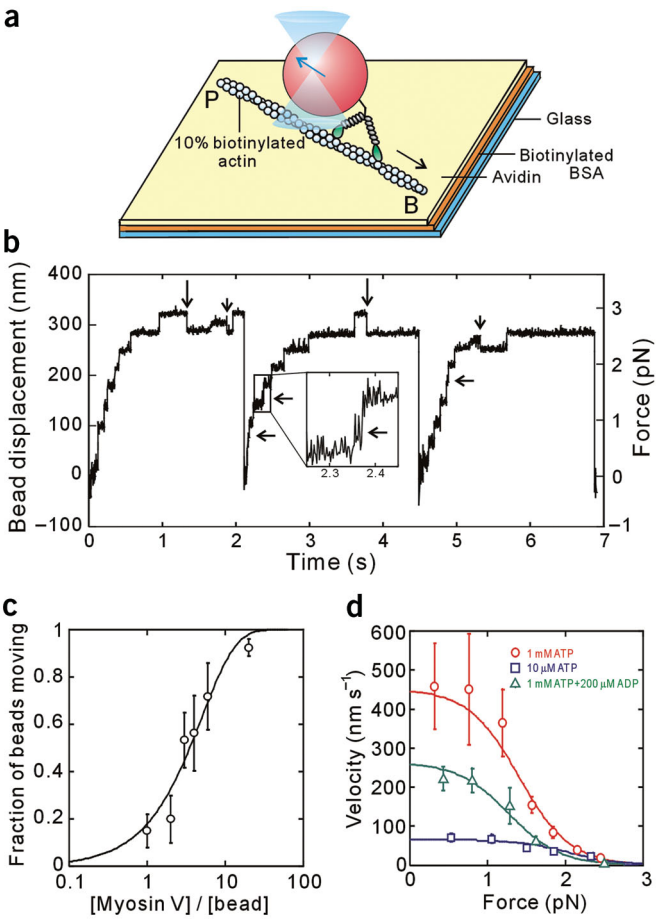

Figure 1 Stepwise movement of single myosin V motor under various external loads. (**a**) Schematic illustration showing how the movement of a myosin V–coated bead is measured. To allow the interaction of myosin V with an actin filament, the bead trapped with optical tweezers was moved onto a single actin filament attached to the glass surface through BSA using the biotin-avidin interaction. The position of the trap center was then fixed. The black and blue arrows, respectively, show the directions for the myosin V movement and the applied external load. (**b**) An example showing the displacement of the bead, where the consecutive 36-nm stepwise movements are clearly seen. A backward 36-nm step is shown by a large vertical arrow. A backward step for the substep is shown by a vertical small arrow. An intermediate state (shown by horizontal arrows) after a short step (substep) is sometimes observable; the 36-nm step in the middle trace is enlarged in an inset. The force was calculated from the displacement of the bead from the trap center times trap stiffness (0.009 pN nm^{-1} in **b**; right axis). (**c**) Relation between proportion of beads that moved along an actin filament and a mixing molar ratio of myosin V to beads. The proportion of moved beads (avg. ± s.d.) was obtained by examining three trials for each bead (20 different beads) at each point. A solid curve was obtained by fitting with $1 - e^{-\lambda C}$, where c is the mixing molar ratio of myosin V to beads, and λ (0.197) is the fitting parameter[9,17,18]. (**d**) Force-velocity relationship obtained under different conditions (n = 8–24 at each point, total = 405). The relationship shown by solid curves was obtained as described in the Methods section.

trap center and immediately began to deviate from the trap center again as a result of the processive motility of myosin V along actin.

We observed regular forward steps of ~36 nm, approximately equal to the half pitch of the actin filament helix. Nearly half of the 36-nm steps contained an 'intermediate state', indicated by horizontal arrows in **Fig. 1b** (compare inset). At higher forces ≥2 pN, backward 36-nm steps (see large vertical arrows in **Fig. 1b**) and backward steps from the intermediate state (see small vertical arrows in **Fig. 1b**) were identified[8,16].

To confirm that a single molecule is sufficient to generate the movement observed, we examined the fraction of beads that bind and move processively along an actin filament at various mixing ratios of myosin V and bead. We confirmed by statistical analysis that single myosin V molecules were sufficient to move the beads (**Fig. 1c**)[17,18].

The force-velocity relationships in the presence of 1 mM ATP (± ADP) were sigmoidal, showing a steep decrease in the velocity at higher than ~1 pN (**Fig. 1d**). In comparison, the relationship in the presence of 10 μM ATP showed a small force dependence. ADP release is rate limiting in the presence of 1 mM ATP[12], whereas ATP binding becomes rate limiting at low ATP concentrations[12]. The present results suggest that ADP release is more load dependent than ATP binding. It should be noted that the stall force, 2.5–3 pN, does not depend on the nucleotide conditions (**Fig. 1d**).

Measurement of substeps within each 36-nm step

The time course of bead movement examined on an expanded time scale with 0.1-ms time intervals clearly shows the existence of substeps within the regular 36-nm step (**Fig. 2**). We identified the presence of

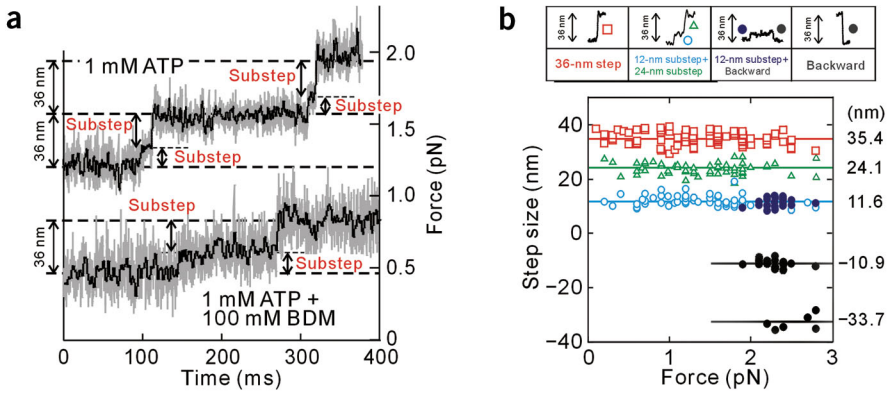

Figure 2 The time course of myosin V movement at a 10-kHz sampling rate and force dependence of the occurrence of various steps. (**a**) Consecutive two substeps at 1 mM ATP shown in the upper trace and at 1 mM ATP + 100 mM BDM shown in the lower trace. We determined whether or not substeps were present by obtaining the histogram of the bead positions at 0.1-ms time intervals (gray lines). Black lines were obtained by the smoothing of 21 successive points. (**b**) Force dependence of step size in the presence of 1 mM ATP. The size of the steps was estimated as described in Methods. The first 12-nm substep, blue circle; the second 24-nm substep, green triangle; the 36-nm step in which substeps could not be identified, red square; the 12-nm substep that was followed by a backward step, dark blue circle; the backward steps, black circles. We could not determine the occurrence of the 24-nm backward step. The figures along the right ordinate are the average step size estimated independent of force as shown by a straight line parallel to the abscissa.

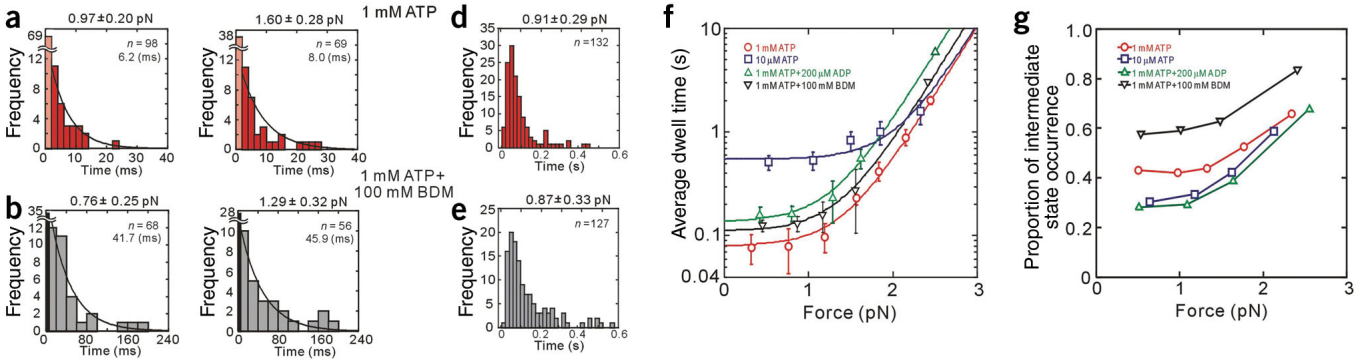

Figure 3 Force dependence of the intermediate and the main dwell times at various nucleotide states and of the occurrence frequency of the intermediate state. (**a**,**b**) Histogram showing the distribution of the dwell time, τ, of the intermediate state in the presence of 1 mM ATP in **a** and 1 mM ATP + 100 mM BDM in **b** at different force levels. The data <2 ms dwell time (pink bars in **a** and thin black bars in **b**) include those in which substeps could not be identified. The fitting curves (thin lines) expressed by $\exp(-\tau / \tau_0)$ were obtained without the data <2 ms (see text for explanation), where τ_0 is a time constant (equal to average dwell time) dependent on developed force. (**c**) Force dependence of the average dwell time, τ_0, of the intermediate state at 1 mM ATP, 10 μM ATP, 1 mM ATP + 200 μM ADP and 1 mM ATP + 100 mM BDM (n = 8–14 at each point, total = 225). The average dwell time was determined at several force levels different from those shown in **a** and **b**. Among the data shown in **a** and **b**, only the data in which the substeps were identified were used for the analysis in **c**. A red line was determined for the data at the first three conditions and a black line for the last condition by using a global fit analysis assuming the same slope for the two lines. (**d**,**e**) Histogram showing the distribution of the main dwell time, τ, in the presence of 1 mM ATP in **d** and 1 mM ATP + 100 mM BDM in **e** at low force level. (**f**) Force dependence of the average dwell time, τ_0 (= $k_1^{-1} + k_2^{-1}$) of the main state at 1 mM ATP, 10 μM ATP, 1 mM ATP + 200 μM ADP and 1 mM ATP + 100 mM BDM (n = 18–32 at each point, total = 562). The average dwell time was determined at several force levels different from those shown in **d** and **e**. All the data shown in **d** and **e** were used for the analysis in **f**. The force dependence of τ_0 for each condition was expressed by $\tau_D \exp(Fd_D / k_BT) + \tau_C$, where τ_C is the time constant representing the dwell time independent of force. The values obtained are summarized in **Table 1**. (**g**) The occurrence frequency of the intermediate state at several force levels for each nucleotide condition. Not only the 36-nm steps with substeps but also those without substeps are included in the first column shown by pink and thin black bars in **a** and **b**. Thus, the occurrence frequency of the 36-nm main steps without substeps was estimated by subtracting that obtained by extrapolating the exponential function of the dwell time distribution for the intermediate state.

the intermediate state by making a histogram of the bead position before and after each 36-nm step. We refer to each 36-nm step, in which substeps could not be identified, as a 'main step'. The state populated after the main step or subsequent to the intermediate state is termed a 'main state'. The intermediate state had a lifetime of a few milliseconds at low forces in the presence of 1 mM ATP (an upper trace in **Fig. 2a**) and tens of milliseconds in the presence of 100 mM BDM (lower trace in **Fig. 2a**). The main state had a longer lifetime (several tens of milliseconds) than the intermediate state in all the conditions tested. The substeps occurred at random and did not correlate with the occurrence of the 36-nm main steps.

The step size was determined directly from the time course of stepwise movements of the myosin V–coated bead. A step size distribution had peaks at 11.6 nm (12-nm substep), 24.1 nm (24-nm substep) and 35.4 nm (36-nm step in which substeps could not be identified), and included backward steps at 12 nm and 36 nm (**Fig. 2b**). The step size of either the two substeps or for the single main step depended little on the force level (**Fig. 2b**), although a possibility that the step size depends on the force level cannot be excluded because we did not take account of the attenuation factor to estimate the step size (see Methods). On the other hand, approaching the stall force, the occurrence frequency of 24-nm and 36-nm steps decreased and that of backward steps increased.

Characterization of the intermediate state

Histograms showing the distribution of intermediate state dwell times under several nucleotide and force conditions fit single exponentials regardless of the nucleotide conditions (**Fig. 3a**,**b**), indicating that this dwell time is coupled with a single chemical reaction. The decay time estimated by exponential fitting became longer as force (balanced to external load) increased. It should be noted here that the occurrence frequency <2 ms dwell time (shown by pink bars in **Fig. 3a** and thin black bars in **Fig. 3b**) largely exceeded that estimated from the exponential fitting of the dwell time, strongly suggesting that there is a pathway for the 36-nm main step without the intermediate state. In the Discussion, we attempt to construct a walking model that can explain this postulate.

The intermediate dwell time did not depend on the concentrations of ATP and ADP (**Fig. 3c**), suggesting that the intermediate state is not coupled with nucleotide binding or release. On the other hand, BDM markedly prolonged the intermediate dwell time (**Figs. 2a** and **3b**).

The force dependence of the average dwell time of the intermediate state is expressed by the single exponential function of the force, $\tau_i \exp(Fd_i / k_BT)$, where τ_i is the average dwell time in the absence of force (F), d_i the characteristic distance (a parameter having the dimension of length that characterizes the bond instability against applied load), k_B the Boltzmann constant and T the absolute temperature (**Fig. 3c**). We determined the values of τ_i and d_i by global fitting of all the data[19,20], assuming that τ_i is only prolonged by the addition of BDM and d_i is common to all the conditions examined (see **Table 1**).

Characterization of the main state

In contrast to the intermediate dwell time (**Fig. 3a–c**), the histogram of the main dwell time (**Fig. 3d**,**e**) shows a peak. The main dwell time can be expressed by the sum of two exponential functions as shown previously[8], indicating that the main dwell time is coupled with two consecutive chemical reactions.

Table 1 Parameters obtained by dwell time analysis

	$\tau_{Total} = \tau_D \exp(Fd_D / k_BT) + \tau_C + \tau_i \exp(Fd_i / k_BT)$			
Nucleotide states	τ_{Total} ($F = 0$)	τ_D (ms), d_D (nm)	τ_C (ms)	τ_i(ms), d_i (nm)
1 mM ATP	86.7 ± 13.0	1.1 ± 0.3, 12.5 ± 0.4	79.7 ± 11.5	5.9 ± 1.2, 2.2 ± 0.2
1 mM ATP + 100 mM BDM	141.2 ± 16.2	1.7 ± 0.4, 12.5 ± 0.4	110.6 ± 9.2	28.9 ± 6.6, 2.2 ± 0.2
1 mM ATP + 200 μM ADP	145.5 ± 20.2	2.8 ± 0.3, 12.5 ± 0.4	136.8 ± 18.7	5.9 ± 1.2, 2.2 ± 0.2
10 μM ATP	553.5 ± 50.1	1.1 ± 0.3, 12.5 ± 0.4	546.5 ± 48.6	5.9 ± 1.2, 2.2 ± 0.2

The main dwell time was fit to the sum of a force-dependent exponential and a constant, whereas the intermediate dwell time was fit to a force-dependent single exponential. The values of parameters τ_D, d_D, τ_C, τ_i and d_i were determined by global fit with nonlinear optimization[19,20] using SigmaPlot 8.0. For the global fit analysis, we assumed that the values of d_D and d_i are common to the main and intermediate states, respectively, and τ_D and τ_i for some nucleotide states.

Either lowering the ATP concentration or adding ADP caused an increase in the average dwell time, τ_0 ($\tau_0 = k_1^{-1} + k_2^{-1}$) (**Fig. 3f**). This indicates that ATP binding and ADP release shorten the dwell time of the main state[8]. We also confirmed that the average dwell time increases with force (**Fig. 3f**). We observed that 100 mM BDM prolonged this dwell time at every force level.

The force (F) dependence of the average main dwell time is expressed by $\tau_D \exp(Fd_D / k_BT) + \tau_C$, where the values of τ_D, d_D and τ_C were determined by global fitting of all the data[19,20], assuming that d_D is common to all the conditions examined, τ_D is longer in the presence of either ADP or BDM, and τ_C is different at every condition. We conclude that τ_D is attributable to ADP release in the absence of load, because the value of τ_D is determined independent of the ATP concentration but prolonged by ADP and BDM (see **Table 1**). τ_C is a constant term, which increased on lowering the ATP concentration and adding ADP (see **Table 1**). Also, it is to be noted that the large value of d_D (12.5 nm) indicates that ADP release largely depends on the force level. (Note that this factor becomes predominant at the force level higher than ~1 pN in 1 mM ATP or ~2 pN in 10 μM ATP, as observed in **Fig. 3f**.)

Frequency of the intermediate state

The occurrence frequency of the intermediate state within the 36-nm main step is greatest in the presence of BDM and is increased with force irrespective of the nucleotide condition (**Fig. 3g**). In the absence of BDM, the proportion merged at a high force level irrespective of the nucleotide conditions, whereas at a low force level the proportion was decreased on lowering the ATP concentration and by the addition of ADP.

Effects of BDM on the ATPase kinetics of myosin V

Actin filaments activate the steady-state ATPase activity of MV-1IQ (**Fig. 4a**). The solid line in **Fig. 4a** is the best fit to a hyperbola (rate = (V_{max} × [actin] / (K_{ATPase} + [actin])). In the absence of BDM, the maximum turnover rate, V_{max}, was 13.7 ± 0.9 s^{-1} and the K_{ATPase} was 3.5 ± 0.6 μM, in agreement with earlier determinations[12,21,22]. BDM (100 mM) reduces the V_{max} and K_{ATPase} approximately two-fold to 6.9 ± 0.2 s^{-1} and 2.3 ± 0.2 μM, respectively. In agreement with an earlier study[23], ~10 mM BDM has no appreciable effect on the maximal steady-state cycling of MV-1IQ.

Actin filaments accelerate the rate of transient P_i release from MV-1IQ-ADP-P_i (**Fig. 4b**). Time courses of P_i release follow single exponentials (**Fig. 4b** inset) because myosin V is limited to a single ATP turnover by including excess ADP in the actin filament solution (see Methods). In the absence of BDM, the maximum rate of P_i release from MV-1IQ-ADP-P_i (k_{+4}' following nomenclature of ref. 24) was 60 ± 9 s^{-1} and the actin concentration at the half-maximum rate (K_9^{-1}, ref. 24) was 7.3 ± 0.6 μM. The rate of myosin V-ADP-P_i binding

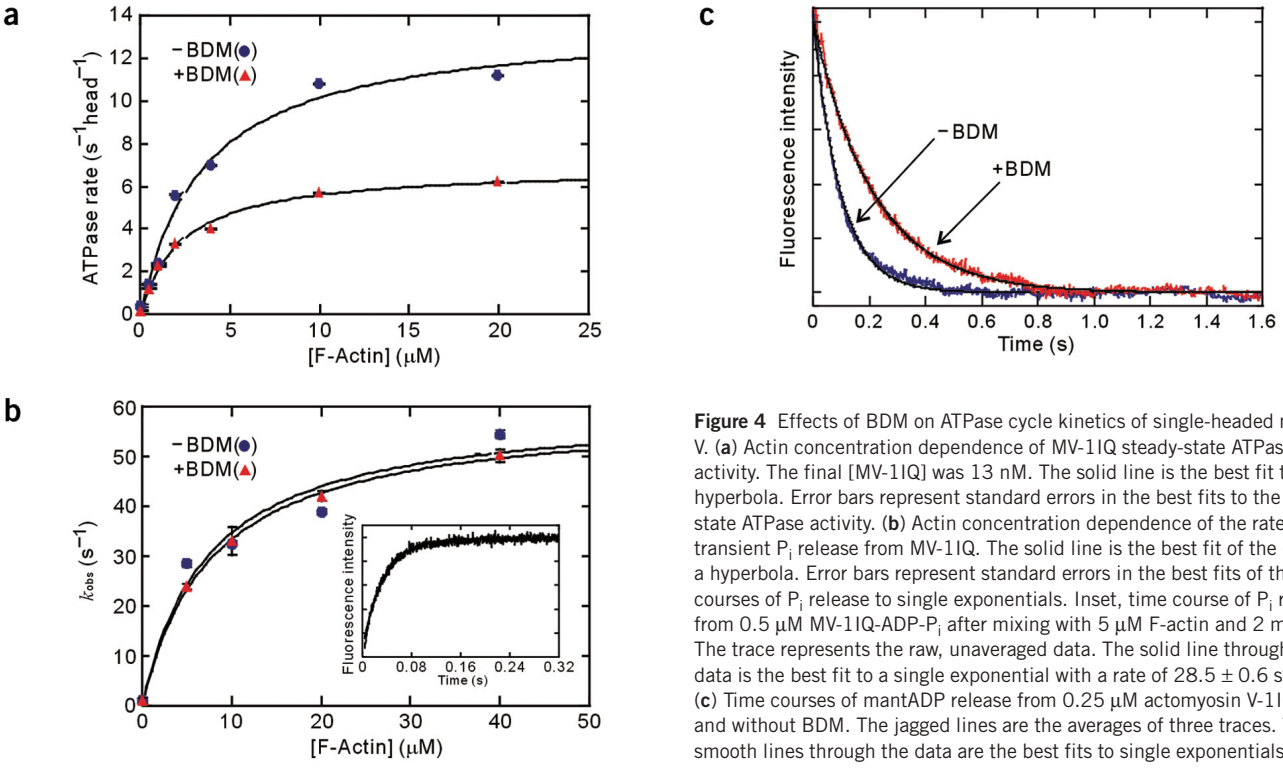

Figure 4 Effects of BDM on ATPase cycle kinetics of single-headed myosin V. (**a**) Actin concentration dependence of MV-1IQ steady-state ATPase activity. The final [MV-1IQ] was 13 nM. The solid line is the best fit to a hyperbola. Error bars represent standard errors in the best fits to the steady-state ATPase activity. (**b**) Actin concentration dependence of the rate of transient P_i release from MV-1IQ. The solid line is the best fit of the data to a hyperbola. Error bars represent standard errors in the best fits of the time courses of P_i release to single exponentials. Inset, time course of P_i release from 0.5 μM MV-1IQ-ADP-P_i after mixing with 5 μM F-actin and 2 mM ADP. The trace represents the raw, unaveraged data. The solid line through the data is the best fit to a single exponential with a rate of 28.5 ± 0.6 s^{-1}. (**c**) Time courses of mantADP release from 0.25 μM actomyosin V-1IQ with and without BDM. The jagged lines are the averages of three traces. The smooth lines through the data are the best fits to single exponentials.

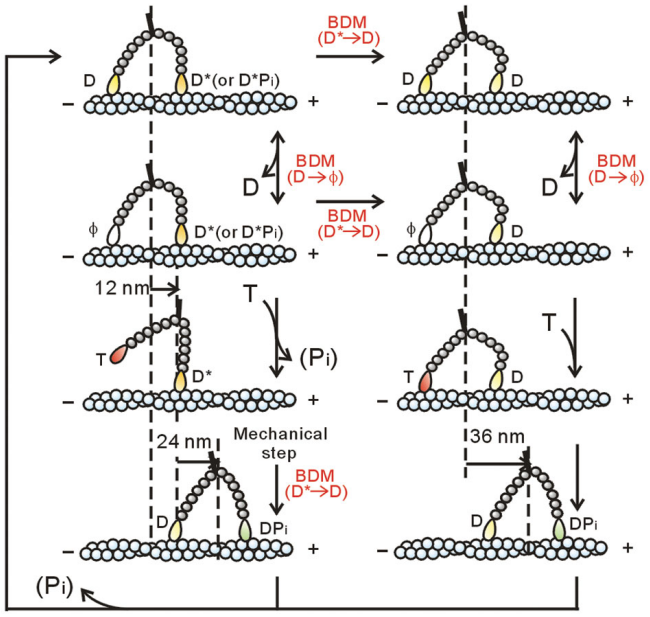

Figure 5 Hand-over-hand model coupled with nucleotide states explaining the present results. We propose that there are two possible pathways: pathway 1 in which 12-nm and 24-nm substeps occur (left column), and pathway 2 in which only the 36-nm main step occurs (right column). BDM is assumed to stabilize both the AMD complex (D) and the AM*D complex (D*), so that the transition rates indicated by red arrows are slowed down. T, ATP; D, ADP; P_i, inorganic phosphate; ϕ, no nucleotides; (P_i), a possible step at which P_i release occurs. For more details, see the text.

to actin filaments (K_9k_{+4}') was ~8 μM^{-1} s^{-1}, comparable to earlier measurements[12]. In the presence of 100 mM BDM, k_{+4}' was 59 ± 1.4 s^{-1} and K_9^{-1} was 7.7 ± 0.6 μM. BDM (100 mM) does not affect k_{+4}' or K_9^{-1} (**Fig. 4b**).

ADP release limits steady-state cycling of myosin V[12,21]. The rate of *N*-methylanthraniloyl-ADP (mantADP) release from actoMV-1IQ in the absence of BDM (**Fig. 4c**) was 10.2 ± 0.1 s^{-1}, in agreement with earlier determinations[12,21,22]. BDM (100 mM) slowed the rate of mantADP release approximately two-fold to 4.6 ± 0.1 s^{-1}. The reduction in ADP release accounts for the slower turnover rate in the presence of 100 mM BDM.

The K_{ATPase} of a myosin with rate-limiting ADP release ($k_{+5}' = V_{max}$) can be related to the maximum rate of P_i release (k_{+4}'), the actin concentration needed to reach half of the maximum P_i release rate (K_9, in units of M^{-1}), and the equilibrium constant for ATP hydrolysis (K_3)(ref. 21): $K_{ATPase} = k_{+5}'(K_9/k_{+4}')$ ($\{1 + K_3\}/K_3$). The two-fold reduction of ADP release (k_{+5}') by 100 mM BDM accounts for the two-fold reduction in V_{max} and K_{ATPase}, suggesting that BDM does not greatly affect the equilibrium constant for ATP hydrolysis (K_3), even though it was not measured directly. This result is in contrast to the case of muscle myosin II, where BDM stabilizes the actomyosin ADP-P_i state and accordingly suppresses P_i release[25]. Finally, we confirmed that the velocity of bead movement in the absence of external load decreased as the concentrations of BDM increased in the presence of 1 mM ATP. The BDM concentration dependence of the average bead velocity showed that the velocity decreases to nearly half with the addition of 100 mM BDM (data not shown). These results are consistent with those of the steady-state ATPase (**Fig. 4a**).

DISCUSSION

We propose here a hand-over-hand walking model of myosin V by taking into account all the experimental data described here together with those reported elsewhere[7,26,27].

First, considering that BDM reduces the rate of ADP release from actomyosin V (**Fig. 4c**) and largely prolongs the intermediate state (**Fig. 3a–c**), it is possible that the main species of the intermediate state is the actomyosin V–ADP complex and that the 24-nm substeps occur accompanied by the ADP release. However, this contradicts the observation that exogenous ADP does not affect the dwell time of the intermediate state. To resolve this apparent contradiction, we assume that isomerization exists in the actomyosin V (AM)–ADP complex, that is, AM*ADP (D*) and AMADP (D). It has already been proposed on the basis of a kinetic study using mant-nucleotides[13] that two states exist in the AM-ADP complex. Furthermore, it is well known that such an isomerization exists in the contraction mechanism of the muscle actomyosin II system[28]. Here, D is a complex produced by the binding of ADP to AM, whereas D* is produced after the hydrolysis of ATP on the AM-ATP complex[28,29]. We assume that D* is the major component of the intermediate state, implying that BDM stabilizes the D* state.

The intermediate state is terminated by the 24-nm substep, so that a straightforward deduction from such consideration is that the 24-nm substep occurs by the mechanical step mainly following the transition from D* to D (a part of the 24-nm substep may be attributable to the binding of detached head (T or DP_i) to actin after Brownian motion). It is notable that one set of researchers[30] showed that, in a single-headed myosin V, there exist two stable binding modes with different angles of the neck region in the ADP-bound state. Also, another group[31] recently showed that a one-headed myosin V produces a 25-nm working stroke.

The occurrence frequency of the 36-nm main step, in which the intermediate state could not be identified, was substantially larger than that predicted from the frequency extrapolated from the exponential fitting of the distribution of the dwell time of the intermediate states (**Fig. 3a,b**). This is understandable if we assume that there are two kinetic pathways for the 36-nm steps with (pathway 1) and without (pathway 2) passing through the intermediate state.

On the main state, the dwell time is largely prolonged on lowering the ATP concentration, and by adding ADP or 100 mM BDM (**Fig. 3d–f**), implying that it is shortened by the attachment of ATP and the detachment of ADP. The simplest assumption deduced from these results is that the main state is terminated; that is, the 12-nm substep occurs upon the ATP binding to a bound trailing head of myosin V from which ADP has been released. This assumption is similar to that predicted by Kolomeisky and Fisher[32] and also consistent with several models previously proposed for myosin V[7,22,24,26,27] and for myosin VI[24]. This is also consistent with the effect of BDM that slows the ADP release (**Fig. 4c**) and the overall ATPase activity as shown by the decrease in the velocity of myosin V movement (data not shown). That is, BDM stabilizes not only the D* state but also the D state.

Thus, we propose the hand-over-hand model as illustrated in **Fig. 5**, which incorporates the previous models[7,26,27] and which can explain, at least qualitatively, all the data presented here. First, the model can account for the existence of two kinds of steps: the 36-nm step composed of the sequential 12-nm and 24-nm substeps (pathway 1), and the 36-nm main step without substeps (pathway 2). The occurrence frequency of these two pathways depends on the conditions as discussed later. According to this model, the intermediate state is in a single-headed binding, whereas the main state is in a double-headed binding. This may be experimentally confirmed by the measurements of the stiffness of the protein-bead complex. In this respect, it is notable

that Veigel *et al.*[31] reported that the low stiffness intervals, which may imply the single-headed binding, exist during the main steps.

Second, the 12-nm substep is assumed to occur upon the binding of ATP to the bound trailing head. Although we do not know whether the bound leading head is D* or D*P_i at this stage (the upper left in **Fig. 5**), we infer that the 12-nm step may be attributable to the conformational change of the leading head due to the transition from DP_i to D* (or D*P_i).

Third, if the transition rate from D* to D decreases on increasing the force level, not only the dwell time of the intermediate state but also that of the main state are prolonged. Besides, we can understand that the higher the force level, the higher the occurrence frequency of the intermediate state irrespective of the nucleotide conditions (**Fig. 3g**), because the transition probability of the process shown by the horizontal arrows in **Fig. 5** (from the pathway 1 to the pathway 2) is suppressed irrespective of the nucleotide conditions.

Fourth, because we assumed that BDM stabilizes not only the D* state but also the D state, both the intermediate state and the main state are stabilized, so that the dwell times of both states are expected to be prolonged. This assumption can also explain a large degree of extension of the dwell time, τ_i, of the intermediate state, because it is tightly coupled to the lifetime of the D* state, whereas the degree of extension of the dwell time of the main state was less because several other states must be involved in the main state.

Fifth, at low ATP concentrations, the attachment of ATP to the bound trailing head is slowed down, so that the probability increases that the transition from D* to D occurs at the bound leading head before ATP binds to the trailing head. This results in the increase in the occurrence frequency of the pathway 2. In the pathway 2, it is expected that the internal strain is largest within the D-D complex, because the leading head is considered to take the orientation similar to that realized after the 24-nm mechanical step. Thus, the D-D (also ϕ-D) complex may have a telemark shape as observed by electron microscopy[7]. It is to be stressed that the two pathways are not independent of each other, but the pathway 1 (or 2) is chosen when the transition from D* to D occurs after (or before) the 12-nm substep; that is, the model in **Fig. 5** proposes that the timing of the 12-nm substep and the isomerization (the transition from D* to D) determines the pathways.

Finally, if the binding affinity of ADP for the bound trailing head is lower than that for the bound leading head because of the mechanochemical coupling due to the internal strain, ADP tends to detach from the bound trailing head, which results in the binding of ATP to the trailing head. Such an asymmetrical binding affinity of ADP may be prerequisite for the directional movement of myosin V toward the barbed end of an actin filament, although this must be experimentally confirmed. We infer that the loading-direction dependency of binding affinity of ADP assumed for myosin V is the reverse of that for kinesin as recently reported by us[20]. Also, another study[33] showed that the binding of ATP to the bound leading head is prerequisite for the directional movement of kinesin toward the plus-end of a microtubule. The correspondence between internal strain and nucleotide affinity in mechanochemical coupling for myosin V may be different from that for kinesin.

METHODS

Protein and assays used for optical trapping measurements. Myosin V was purified from chick brains[34]. Actin purified from rabbit skeletal muscle was biotinylated by 10% and, after polymerization, the filaments were labeled with rhodamine phalloidin (Molecular Probes)[35]. About 1 nM of fluorescent polystyrene beads (200 nm in diameter, yellow-green; Molecular Probes) were incubated for 20 min in an assay buffer (10 mM imidazole-HCl, pH 7.2, 75 mM KCl, 2.5 mM $MgCl_2$, 2 mM DTT and 0.1 mM EGTA) containing 10 mg ml^{-1} BSA. Myosin V (650 kDa) molecules were mixed with the beads at a molar ratio of 3:1 in assay buffer containing 300 mM KCl instead of 75 mM KCl as had been used in the previous studies. The average number of functional myosin V molecules on a bead was estimated by statistical analyses to be one (considering the geometry of the myosin V on the bead, we estimate that only single myosin V molecules interacted with an actin filament in almost all the measurements[17,20]). Assay buffer containing biotinylated BSA at 3 mg ml^{-1} was introduced into a flow cell and incubated for 2 min to coat the glass surface with biotinylated BSA. After rinsing with two volumes of assay buffer, 2 mg ml^{-1} streptavidin in assay buffer was flowed into the cell and incubated for 2 min. After rinsing with assay buffer, a solution of actin filaments, of which 10% was biotinylated and labeled with rhodamine-phalloidin, was flowed into the cell to allow binding of the filaments to the glass surface through avidin-bound biotinylated BSA. The flow cell was then filled with assay solution containing the myosin V–coated beads, filtered BSA and an oxygen-scavenging enzyme system[9]. The final solvent condition was approximately 0.1 pM myosin V–coated beads, 10 mM imidazole-HCl, pH 7.2, 75 mM KCl, 2.5 mM $MgCl_2$, 2 mM DTT, 0.1 mM EGTA, 3.6 mg ml^{-1} glucose, 0.08 mg ml^{-1} glucose oxidase, 0.01 mg ml^{-1} catalase, 0.95% (v/v) β-mercaptoethanol and nucleotides (1 mM ATP, 10 μM ATP, 1 mM ATP + 200 μM ADP or 1 mM ATP + 100 mM BDM). We were able to observe repeatedly the stepwise movements of myosin V–coated beads along the same actin filaments on the same beads, presumably for the same myosin V molecules, by using optical tweezers to manipulate the beads. All experiments on microscopy were done at 24 ± 1 °C.

We found that the percentage of biotinylation of actin is important for the processive movement of myosin V. In other words, myosin V could move processively on 1% and 10% biotinylated actin filaments, whereas it could not on 100% biotinylated ones, suggesting that the manner in which actin filaments bind to the glass surface is crucial. It should be noted that myosin V is reported to be a left-handed spiral motor[9], so that the revolution of a myosin V–coated bead around the actin filament could be sterically hindered. However, this possibility could be ignored, because the maximum distance of bead displacement was less than ~0.3 μm (**Fig. 1b**), such that it was much shorter than the distance, 2 μm, for one revolution[9].

The velocity of myosin V under no external load was obtained from the time course of bead movement along an actin filament in the absence of optical trap. The bead position was determined by the center of the fluorescence intensity distribution of the bead every video frame.

Proteins and reagents used for biochemical experiments. Actin was purified from rabbit skeletal muscle and gel filtered over Sephacryl S-300HR (ref. 12). The motor domain of myosin V containing the first IQ motif (MV-1IQ) and the essential light chain, LC-1sa, were co-expressed in Sf9 insect cells and purified by FLAG affinity chromatography[12]. The fluorescently labeled mutant of the phosphate-binding protein (MDCC-PBP; clone provided by M.R. Webb, National Institute for Medical Research, London) was expressed, purified and labeled as described[36]. ATP and ADP were purchased from Roche Molecular Biochemicals. mantADP was synthesized as described[37] or purchased from Molecular Probes with identical results. A molar equivalent of $MgCl_2$ was added to nucleotides immediately before use. BDM was purchased from Sigma (lot 092K1722) and prepared as a 250 mM stock solution in KMg50-MOPS (10 mM MOPS, pH 7.0, 50 mM KCl, 1 mM $MgCl_2$, 1 mM EGTA and 1 mM DTT) immediately before use[21].

Instrumentation and calibration. The myosin V–coated bead was trapped with an optical tweezers—that is, a focused infrared laser beam (λ = 1,064 nm, 2 W; Spectra Physics)—and illuminated diagonally by a focused red laser beam (λ = 685 nm, 20 mW; Phototechnica) through an objective lens (fluor ×100/1.3 oil; Nikon). The light scattered by the bead was gathered by an objective lens with an aperture (NA = 0.5, ×100 oil; Olympus) and projected onto a quadrant photodiode sensor (S4349; Hamamatsu Photonics) coupled to a differential amplifier (20-kHz roll-off frequency; OP711, Sentec). The fluorescently labeled beads and actin labeled with rhodamine-phalloidin were excited by a green laser (λ = 532 nm, 50 mW; Peace Engineering), and the fluorescence images were captured by a silicon-intensified target camera (C-2740; Hamamatsu Photonics) and displayed on a video monitor. The bead positions were

recorded on a computer equipped with a laboratory interface board (MacLab; AD Instruments)[15] at a sampling rate of 10 kHz through a digital low-pass filter at 10 kHz. The bead displacement was calibrated by moving the photodiode[15]. The trap stiffness of the optical tweezers was calibrated for every bead from the standard deviation of the position fluctuation of the trapped bead (0.009–0.011 pN nm^{-1}). The step size was obtained directly from individual stepwise movements of the bead at a sampling time of 0.1 ms and estimated as the difference between the average bead positions determined for 5 ms each interval just before and after the steps. We did not take into account the attenuation factor, which is a function of the stiffness of optical trap and the stiffness of the protein-bead complex[15,17], because the trap stiffness we used is considered to be much smaller than that of the protein-bead complex. The average velocity of bead movement (v) was estimated by dividing the average step size (36 nm) by the average total dwell time (τ_{Total} in units of ms) at each external load, which is balanced to the force (F) generated by myosin V. Force-velocity relationships were described by the following function: $v = 36 \text{ nm} / \tau_{Total} = 36/\{\tau_D \exp(Fd_D / k_BT) + \tau_C + \tau_i \exp(Fd_i / k_BT)\}$ (nm ms^{-1}), where τ_D, d_D, τ_C, τ_i, d_i, k_B and T are described in the text.

Steady-state and transient kinetic experiments. All kinetic experiments were done at 25 ± 0.1 °C in KMg50-MOPS with an SX.18MV-R stopped-flow apparatus (Applied Photophysics). Fitting was done with Pro-K software provided with the instrument. Steady-state ATPase activity of MV-1IQ was measured using the ATP-regenerating, NADH-coupled assay as described[21]. BDM had minimal effects on the assay components as determined by direct mixing with MgADP.

Transient P_i release of MV-1IQ was measured using MDCC-PBP (λ_{ex} = 430 nm, 455 nm emission filter) with the instrument in sequential mixing mode as described[24]. Briefly, 2 μM MV-1IQ (treated with 0.01 U ml^{-1} potato grade VII apyrase to remove residual ADP and ATP, ± 200 mM BDM) was mixed with 300 μM MgATP (± 200 mM BDM) and aged for 40–60 ms to allow for nucleotide binding and hydrolysis to occur, then mixed with an equal volume of a range of actin filament concentrations. As first described for myosin VI[24], myosin V was limited to a single ATP turnover by including 2 mM MgADP with the actin. ADP competes with ATP for binding to myosin V after the first turnover and inhibits subsequent steady-state cycling. Therefore, time courses follow single exponentials (see **Fig. 4b** inset) rather than exponentials followed by a linear steady-state component, permitting more accurate fitting of the P_i release time courses. This method of measuring P_i release can be used for all high-duty-ratio myosins with rapid rates of ADP binding and high ADP affinities.

ADP release was measured with a fluorescent nucleotide mantADP[12]. The fluorescence of mantADP (λ_{ex} = 366 nm, 400-nm emission filter) was monitored after an equilibrated mixture of 0.5 μM actomyosin V-1IQ (± 200 mM BDM) and 20 μM mantADP was mixed with an equal volume of 2 mM MgADP.

ACKNOWLEDGMENTS

We thank M.R. Webb for the phosphate-binding protein clone and suggestions on purification and labeling, and H.L. Sweeney for providing the myosin V heavy and light chain viruses. We are grateful to N. Sasaki, M.Y. Ali, K. Kinosita, Jr. and E.M. Ostap for encouragement and stimulating discussions. This research was partly supported by Grants-in-Aid for Specially Promoted Research, for the Bio-venture Project and for The 21st Century COE Program (Physics of Self-Organization Systems) at Waseda Univ. from the Ministry of Education, Sports, Culture, Science and Technology of Japan (to S.I.) and supported by a Scientist Development Grant from the American Heart Association and a grant from the US National Science Foundation (to E.M.D.L.C.). S.U. is a postdoctoral fellow of the Japan Society for the Promotion of Science. A.O.O. is supported by a Cellular & Molecular Biology graduate training grant (Yale University).

COMPETING INTERESTS STATEMENT

The authors declare that they have no competing financial interests.

Received 31 March; accepted 18 June 2004
Published online at http://www.nature.com/nsmb/

1 Cheney, R.E. *et al.* Brain myosin V is a two-headed unconventional myosin with motor activity. *Cell* **75**, 13–23 (1993).
2. Miller, K.E. & Sheetz, M.P. Characterization of myosin V binding to brain vesicles. *J. Biol. Chem.* **275**, 2598–2606 (2000).
3. Vale, R.D. The molecular motor toolbox for intracellular transport. *Cell* **112**, 467–480 (2003).
4. Reck-Peterson, S., Provance, D.W., Mooseker, M.S. & Mercer, J.A. Review: class V myosins. *Biochim. Biophys. Acta* **1496**, 36–51 (2000).
5. Sakamoto, T., Amitani, I., Yokota, E. & Ando, T. Direct observation of processive movement by individual myosin V molecules. *Biochem. Biophys. Res. Commun.* **272**, 586–590 (2000).
6. Mehta, A.D. *et al.* Myosin V is a processive actin-based motor. *Nature* **400**, 590–593 (1999).
7. Walker, M. *et al.* Two-headed bindings of a processive myosin to F-actin. *Nature* **405**, 804–807 (2000).
8. Rief, M. *et al.* Myosin V stepping kinetics: a molecular model for processivity. *Proc. Natl. Acad. Sci. USA* **97**, 9482–9486 (2002).
9. Ali, M.Y. *et al.* Myosin V is a left-handed spiral motor on the right-handed actin helix. *Nat. Struct. Biol.* **9**, 464–467 (2002).
10. Forkey, J.N., Quinlan, M.E., Shaw, M.A., Corrie, J.E. & Goldman, Y.E. Three-dimensional structural dynamics of myosin V by single-molecule fluorescence polarization. *Nature* **422**, 399–404 (2003).
11. Yildiz, A. *et al.* Myosin V walks hand-over-hand: single fluorophore imaging with 1.5-nm localization. *Science* **300**, 2061–2065 (2003).
12. De La Cruz, E.M., Wells, A.L., Rosenfeld, S.S., Ostap, E.M. & Sweeney, H.L. The kinetic mechanism of myosin V. *Proc. Natl. Acad. Sci. USA* **96**, 13726–13731 (1999).
13. Trybus, K.M., Krementsova, E. & Freyzon, Y. Kinetic characterization of a monomeric unconventional myosin V construct. *J. Biol. Chem.* **274**, 27448–27456 (1999).
14. Higuchi, H. & Takemori, S. Butanedione monoxime suppresses contraction and ATPase activity of rabbit skeletal muscle. *J. Biochem.* **105**, 638–643 (1989).
15. Nishiyama, M., Higuchi, H. & Yanagida, T. Chemomechanical coupling of the forward and backward steps of single kinesin molecules. *Nat. Cell Biol.* **4**, 790–797 (2002).
16. Moore, J.R., Krementsova, E.B., Trybus, K.M. & Warshaw, D.M. Myosin V exhibits a high duty cycle and large unitary displacement. *J. Cell Biol.* **155**, 625–635 (2001).
17. Kojima, H., Muto, E., Higuchi, H. & Yanagida, T. Mechanics of single kinesin molecules measured by optical trapping nanometry. *Biophys. J.* **73**, 2012–2022 (1997).
18. Svoboda, K., Schmidt, C.F., Schnapp, B.J. & Block, S.M. Direct observation of kinesin stepping by optical trapping interferometry. *Nature* **365**, 721–727 (1993).
19. Schnitzer, M.J., Visscher, K. & Block, S.M. Force production by single kinesin motors. *Nat. Cell Biol.* **2**, 718–723 (2000).
20. Uemura, S. & Ishiwata, S. Loading direction regulates the affinity of ADP for kinesin. *Nat. Struct. Biol.* **10**, 308–311 (2003).
21. De La Cruz, E.M., Sweeney, H.L. & Ostap, E.M. ADP inhibition of myosin V ATPase activity. *Biophys. J.* **79**, 1524–1529 (2000).
22. De La Cruz, E.M., Wells, A.L., Sweeney, H.L. & Ostap, E.M. Actin and light chain isoform dependence of myosin V kinetics. *Biochemistry* **39**, 14196–14202 (2000).
23. Ostap, E.M. 2,3-Butanedione monoxime (BDM) as a myosin inhibitor. *J. Muscle Res. Cell Motil.* **23**, 305–308 (2002).
24. De La Cruz, E.M., Ostap, E.M. & Sweeney, H.L. Kinetic mechanism and regulation of myosin VI. *J. Biol. Chem.* **276**, 32373–32381 (2001).
25. Herrmann, C., Wray, J., Travers, F. & Barman, T. Effect of 2,3-butanedione monoxime on myosin and myofibrillar ATPases. An example of an uncompetitive inhibitor. *Biochemistry* **31**, 12227–12232 (1992).
26. Spudich, J.A. & Rock, R.S. A crossbridge too far. *Nat. Cell Biol.* **4**, E8–E10 (2002).
27. Vale, R.D. Myosin V motor proteins: marching stepwise towards a mechanism. *J. Cell Biol.* **163**, 445–450 (2003).
28. Goldman, Y.E. and Brenner, B. Special topic: molecular mechanism of muscle contraction. *Annu. Rev. Physiol.* **49**, 629–636 (1987).
29. Dantzig, J.A., Hibberd, M.G., Trentham, D.R. & Goldman, Y.E. Cross-bridge kinetics in the presence of MgADP investigated by photolysis of caged ATP in rabbit psoas muscle fibres. *J. Physiol.* **432**, 639–680 (1991).
30. Burgess, S. *et al.* The prepower stroke conformation of myosin V. *J. Cell Biol.* **159**, 983–991 (2002).
31. Veigel, C., Wang, F., Bartoo, M.L., Sellers, J.R. & Molloy, J.E. The gated gait of the processive molecular motor myosin V. *Nat. Cell Biol.* **4**, 59–65 (2002).
32. Kolomeisky, A.B. & Fisher, M.E. A simple model describes the processivity of Myosin V. *Biophys. J.* **84**, 1642–1650 (2003).
33. Rosenfeld, S.S., Fordyce, P.M., Jefferson, G.M., King, P.H. & Block, S.M. Stepping and stretching. How kinesin uses internal strain to walk processively. *J. Biol. Chem.* **278**, 18550–18556 (2003).
34. Cheney, R.E. Purification and assay of myosin V. *Methods Enzymol.* **293**, 3–18 (1998).
35. Yanagida, T., Nakase, M., Nishiyama, K. & Oosawa, F. Direct observation of motion of single F-actin filaments in the presence of myosin. *Nature* **307**, 58–60 (1984).
36. Brune, M. *et al.* Mechanism of inorganic phosphate interaction with phosphate binding protein from *Escherichia coli*. *Biochemistry* **37**, 10370–10380 (1998).
37. Hiratsuka, T. New ribose-modified fluorescent analogs of adenine and guanine nucleotides available as substrates for various enzymes. *Biochim. Biophys. Acta* **742**, 496–508 (1983).